

Current-induced metastable resistive states with memory in low-doped manganites

Y. Yuzhelevski, V. Markovich, V. Dikovskiy, E. Rozenberg, G. Gorodetsky, and G. Jung*
Department of Physics, Ben Gurion University of the Negev, P.O. Box 653, 84105 Beer-Sheva, Israel

D. A. Shulyatev and Ya. M. Mukovskii
Moscow State Steel and Alloys Institute, 117936 Moscow, Russia
 (Received 8 July 2001; published 26 November 2001)

The influence of dc current flow on the resistivity and phase transitions in low-doped $\text{La}_{0.82}\text{Ca}_{0.18}\text{MnO}_3$ single crystals has been investigated. At low temperatures, where the resistivity strongly increases with decreasing temperature, dc current depresses resistivity in a way consistent with the domination of tunneling-conduction mechanisms. Current flow exceeding some threshold currents results in resistivity switching and metastability. Bipolar current sweep exceeding threshold currents in both positive and negative direction creates low-resistivity states in the sample. The low-resistivity state converts into a very-low- and stable-resistivity state under a stronger bipolar current sweep. Current-induced low-resistivity states are characterized by long-term memory persisting even after storing the sample for a few days at room temperature. The memory can be erased by ac current flow at high temperatures. The results are interpreted in terms of a spin-polarized tunnel conduction mechanism, which modifies phase-separation conditions along the percolation path.

DOI: 10.1103/PhysRevB.64.224428

PACS number(s): 75.25.+z, 71.27.+a, 71.30.+h, 75.50.-y

I. INTRODUCTION

Remarkable magnetic and transport properties of mixed-valence manganese perovskites of the form $R_{1-x}A_x\text{MnO}_3$, where R is a rare-earth ion and A is a divalent ion, continuously attract attention of many research groups.^{1,2} The central feature is a huge decrease in resistivity by application of the magnetic field, referred to as the colossal magnetoresistance (CMR) effect. Physical properties of CMR manganites are very sensitive to external perturbations. Phase-transition temperatures are modified by application of magnetic and electric fields, pressure, current bias, illumination with light, or x rays. While magnetic field and pressure change global properties of a CMR sample, the influence of light, x rays, and current may not always result in a global bulk phase transition. Local metal-insulator (MI) phase transitions may lead instead to nucleation of filamentary metallic conducting paths.³ The resulting phase separation (PS) together with the percolation conductivity is an intrinsic feature of doped manganites and it may even lie at the very core of the CMR phenomenon.

Spectacular manifestations of electric-field effects in perovskite manganites take the form of colossal electroresistance⁴⁻⁷ effect and strong, orders of magnitude high, current-induced abrupt resistivity jumps.⁵⁻⁷ The majority of studies of electric-field effects in CMR manganites were performed using charge-ordered samples involving current injection into highly conducting filamentary paths.⁴⁻⁸ The conductivity in such systems is strongly non-Ohmic and as a rule increases with increasing current, eventually leading to a collapse of the insulating charge-ordered state, insulator-metal phase transition, and appearance of metallic-like conductivity in the ferromagnetic state.⁷ The metallic conductivity persists even after lowering of the applied bias; the system exhibits the conductivity memory effect.⁸

Doped CMR manganites have been most intensively stud-

ied in the optimum doping concentration range $0.2 < x < 0.5$, corresponding to the metallic ferromagnetic (FM) ground state. The low-doping regime has been much less explored. Since the onset of the metallic conductivity occurs above a certain critical concentration x_c , a subtle competition between charge-carrier motion and magnetic spin and orbital moments in lightly doped manganites leads to intrinsic phase separation associated with MI transition and, consequently, to the percolation conductivity.⁹ As confirmed by numerous experiments the magnetic phase of $\text{La}_{1-x}\text{Ca}_x\text{MnO}_3$ (LCMO) and $\text{La}_{1-x}\text{Sr}_x\text{MnO}_3$ (LSMO) in the low-doping regime, $x < x_c$, is indeed macroscopically inhomogeneous.¹⁰⁻¹² For Ca concentration between 0.05 and 0.20, the phase-separated state in LCMO becomes a stable ground state at temperatures below T_c .¹⁰⁻¹² The size of PS domains range from 5–20 Å to fractions of a micron.¹³ Since the ferromagnetic metallic regions embedded in the antiferromagnetic insulating matrix are not directly connected, the low-doped LCMO constitutes an antiferromagnetic insulator at low temperatures. It follows from the LCMO phase diagram that concentration $x = 0.18$ of Ca^{2+} ions is very close to the doping level marking a border between inhomogeneous antiferromagnetic and ferromagnetic metallic ground states of the system.¹¹ One expects, therefore, that strong competition between different magnetic interactions should enhance the influence of bias current on transport and magnetic properties of LCMO with $x = 0.18$.

In this paper we report on experiments concerning the electrical-current influence on resistivity of low-doped $\text{La}_{0.82}\text{Ca}_{0.18}\text{MnO}_3$ single crystals. In particular, we demonstrate that the bipolar electric-current ramp develops various metastable low-resistive states. Some of the low-resistivity states are characterized by a long-term memory of their resistivity, which survives even thermal cycling to room temperatures. The results point to a decisive role of the FM clusters and spin-polarized tunneling in the performance of a conductive-percolation network across the sample.

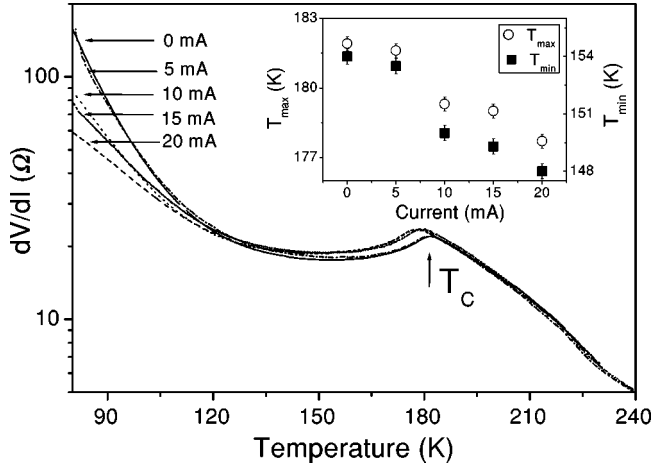


FIG. 1. Temperature dependence of the differential resistivity of $\text{La}_{0.82}\text{Ca}_{0.18}\text{MnO}_3$ single crystal for various applied current biases during the cooling run. Inset shows the dependence of the temperatures of the local resistivity maximum and minimum on current bias.

II. EXPERIMENT AND RESULTS

The experiments were performed with $\text{La}_{0.82}\text{Ca}_{0.18}\text{MnO}_3$ single crystals grown by a floating-zone method, as described elsewhere.¹⁴ As-grown crystals were cut into individual samples for resistive and magnetization measurements. Samples for the resistivity measurements were prepared in the form of $(8 \times 3 \times 1.6)\text{-mm}^3$ bars, having the longest dimension along the $\langle 110 \rangle$ crystalline direction. Current and voltage leads were attached to the pre-evaporated silver contacts by a conducting silver-epoxy bound. Transport measurements of current-voltage characteristics (I - V) and differential resistance ($R_d = dV/dI$) were performed at zero applied magnetic field in a standard four-point arrangement. The separation between the voltage contacts was 2.5 mm. We have used $5 \mu\text{A}$ at 390 Hz low-frequency current modulation for the phase-sensitive lock-in R_d measurements.

Figure 1 shows the temperature dependence of R_d of our crystal during a slow cooling down to liquid-nitrogen temperature using different applied dc currents I_b . All $R_d(T)$ curves demonstrate a shallow bump around $T_s = 225$ K. At temperatures below T_s , the characteristics reach a current-dependent local resistivity maximum. The arrow in Fig. 1 is placed at Curie temperature $T_c = 182 \pm 1$ K, which was determined by independent magnetization measurements.¹⁵ When there is no current flow in the sample the magnetic T_c coincides closely with T_{max} . This allows one to associate the local resistivity maximum with the ferromagnetic phase transition. As shown in the inset to Fig. 1 the increasing current shifts T_{max} to lower temperatures and increases the resistivity seen at T_{max} . Below T_{max} the resistivity initially decreases, reaches a shallow minimum at a current-dependent T_{min} , $T_{min} = 150$ K at $I_b = 0$, and further increases with decreasing temperature. T_{min} decreases with increasing current at a rate that is close to the rate at which T_{max} decreases with current, see inset to Fig. 1.

There is a slight thermal hysteresis between cooling and heating curves around T_{min} . The phase transition around

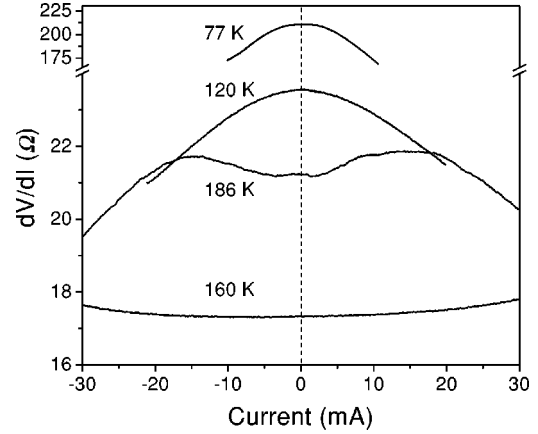


FIG. 2. Differential resistivity of $\text{La}_{0.82}\text{Ca}_{0.18}\text{MnO}_3$ single crystal in a pristine state as a function of current bias at different temperatures.

T_{max} is likely of the second order and displays no hysteresis. Although the hysteresis around T_{min} is much smaller than that seen in other CMR manganite systems, it confirms that lowest-temperature phase transition in CMR materials is of the first order while phase transitions at high temperatures are of the second order.¹⁶

The experiments show that current significantly influences the resistivity only at temperatures below T_{max} . For $T > T_{max}$, the current effect is very weak and all $R_d(T)$ curves in Fig. 1 practically coincide at high temperatures. Within the temperature range $T_{min} < T < T_{max}$ the resistivity slightly increases with current. The most pronounced influence of the bias current on R_d is observed well below T_{min} , where the resistivity strongly decreases with increasing current. The sign of dR_d/dI and its inversion at a temperature close to T_{min} , together with the similarity of dT_{min}/dI_b and dT_{max}/dI_b rates, suggests that the entire effect may be due to a simple Joule heating. The resistivity changes could be trivially attributed to a difference between the measured and the actual temperature of the sample arising from a significant heat dissipation due to the current flow. Before proceeding further we want to address this issue and to demonstrate that the heating mechanism cannot be responsible for the observed resistivity behavior.

There are several arguments that allow us to reject the heating scenario. First of all, the heating effect should be present at all temperatures and not appear only below T_{max} . Furthermore, $R_d(T)$ curves recorded at various I_b are not simply shifted along the temperature axis, as would be expected for the heating effect, which increases with increasing current. The behavior of the local resistivity maximum, a decrease of T_{max} and increase of $R_d(T_{max})$ with current, is also inconsistent with the heating scenario. Finally, the temperature increase associated with the Joule heating should be proportional to the dissipated power. The inset to Fig. 1 demonstrates that this is clearly not the case. Moreover, an apparent rate discontinuity between 5 mA and 10 mA can hardly be reconciled with the heating scenario.

Figure 2 shows the differential resistance as a function of current at several temperatures around and below T_c . At T

=186 K, slightly above T_c , the resistance initially increases with increasing current, but eventually at high currents pronouncedly decreases with current. Symmetrically decreasing bell-shaped $R_d(I)$ curves were recorded at all investigated temperatures below T_{min} , see, e.g., recordings for $T = 120$ K and 77 K. At temperatures close to T_{min} the dynamic resistance is almost current independent, see $R_d(I)$ at 160 K. The characteristics shown in Fig. 2 provide yet another argument against the simple-heating scenario. For temperatures above T_c , where dR_d/dT is negative, the Joule heating should lead to a monotonic decrease of the resistivity with increasing current (increasing dissipated power). However, the predicted behavior is not observed in the experiment, see the 186-K recording. Decrease of R_d with increasing current is observed only at temperatures well below T_c .

At low temperatures, where the resistivity is strongly current dependent, polarization of the sample with dc bias exceeding certain threshold values causes abrupt resistivity jumps and creation of metastable low-resistivity states. Properties and resistance of the metastable states depend in a complex way on the bias history of the sample. In the following we provide a detailed description of the procedures leading to low-resistivity metastable states. All metastable states described in this paper have been created and investigated in the zero-field cooling and zero applied magnetic field.

The smooth bell-shaped curve, labeled 77 K in Fig. 2, represents the pristine resistivity state of our crystal since it has been recorded after a slow cooling down of the sample from room temperature to 77 K with zero bias current. The pristine resistivity is fully reversible with respect to the current and temperature cycling, provided the applied current does not exceed certain threshold values, here roughly corresponding to the current range at which $R_d(I)$ is plotted in Fig. 2 ($\sim \pm 10$ mA). The evolution of the sample resistivity due to application of specific current procedures is illustrated in Fig. 3. The current increase above the first threshold current I_{th1} [about 12.5 mA in Fig. 3(a)] results in an abrupt jump of the resistivity and creation of the first metastable resistivity state (MRS). This MRS is characterized by the appearance of quasiperiodic oscillations in $R_d(I)$ characteristics accompanied by a pronounced resistivity noise with a strong $(1/f)$ -like spectrum. Moreover, at a certain current range the MRS exhibits colossal random telegraph-resistivity fluctuations with bias-dependent lifetimes and telegraph-signal amplitude approaching 10% of the total sample resistance.¹⁷

Further evolution of the MRS depends in a remarkable way on the direction and the range of the current bias. In the record shown in Fig. 3(b) the current has been slowly decreased from the maximum value reached in the preceding up-ramp illustrated in Fig. 3(a). Note that despite the initial hysteresis in the resistivity we actually return to an only slightly distorted smooth bell-like curve, almost identical with the characteristics of the pristine state, in particular, at small currents. The resistance during a subsequent current ramp in the opposite (negative) direction follows the smooth bell-like curve until a pronounced resistance jump appearance at $-I_{th1}$, see Fig. 3(b). At this instant we reverse again

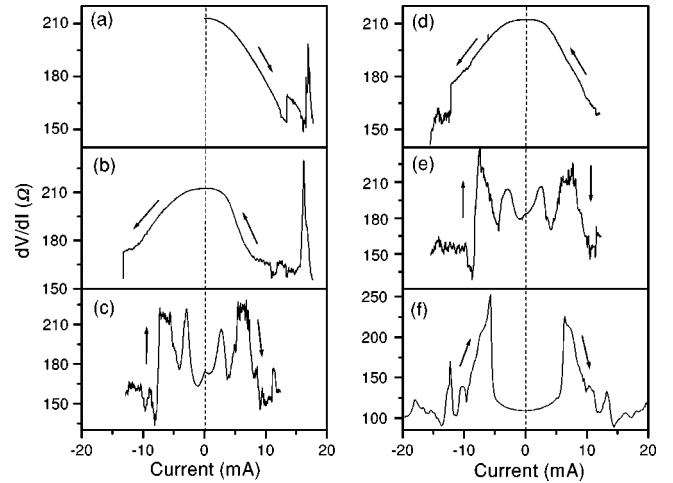


FIG. 3. (a)–(f) The evolution of the differential resistance of LCMO single crystal at $T=77$ K with successive bias current ramps. (a) Initial ramp from $I=0$ to currents above the first threshold current I_{th1} . Note appearance of current-imposed resistivity switching at I_{th1} and following peak structure at higher currents. (b) Subsequent current ramp from $I > +I_{th1}$ to negative currents $|-I| > |-I_{th1}|$ and the return sweep to $I > |I_{th1}|$, shown in (c). Note the formation of the VLRS in (c). (d) Subsequent, return current sweep from $I > +I_{th1}$ to $|-I| > |-I_{th1}|$. (e) The following current ramp from $-I_{th1}$ back to $+I_{th1}$. (f) The $R_d(I)$ characteristics after sweeping to high currents exceeding I_{th2} , more than 30 mA.

the direction of the current sweep and decrease the negative current. The characteristic that follows, see Fig. 3(c), is however markedly different from the previously observed bell-shaped one, indicating that a bipolar current sweep exceeding both the positive and the negative thresholds creates a completely different resistivity state. As shown in Fig. 3(c), with decreasing current we pass through a strongly fluctuating regime, followed by an up-turn of the resistivity to the levels exceeding the maximum R_d seen in the previous recordings at $I_b=0$. Nevertheless, the most striking new feature of this low-resistivity state (LRS) is a deep resistance well at low currents. The resistance at the bottom of the well $R_d(0)$ in the LRS is substantially smaller than the corresponding value in the pristine and MRS state. The well is slightly asymmetric and a small zero-bias anomaly can be seen around $I_b=0$. We have verified that the asymmetry of the well and the zero-bias anomaly are associated with the symmetry of the preceding bidirectional current sweep. When the maximum currents in the negative and positive direction are exactly the same, the asymmetry of the well and zero-bias anomaly disappear.

LRS established at the negative threshold $-I_{th1}$ converts to the previously observed MRS state with distorted bell-shaped characteristics under a current sweep in the opposite (positive) direction above the threshold $+I_{th1}$, as illustrated in Fig. 3(d). The system returns back to LRS after a subsequent negative-direction current sweep exceeding $-I_{th1}$, as shown in Fig. 3(e). However, when one ramps the bias current within the limits imposed by the threshold currents, $|I_b| \leq I_{th1}$, then the state of the system remains unchanged. Exceeding the threshold currents results in a huge resistivity

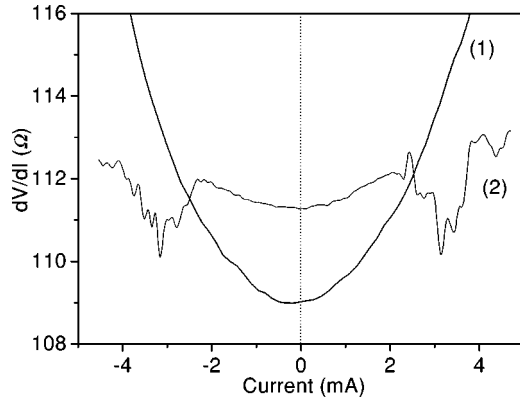


FIG. 4. Differential resistivity of $\text{La}_{0.82}\text{Ca}_{0.18}\text{MnO}_3$ single crystal at 77 K seen at small currents, immediately after the formation of VLRS state [curve (1)] and after the thermal cycling to room temperatures [curve (2)].

hysteresis in which resistivity evolves according to MRS behavior for currents decreasing from $+I_{th1}$ to $-I_{th1}$ and according to LRS for the opposite direction of the current. In this sense, the threshold currents can be recognized as the limiting currents for the reversible hysteresis behavior.

What happens when the current is increased well beyond I_{th1} ? We have found that this results in a creation of yet another low-resistivity state. As illustrated in Fig. 3(f), by sweeping the current in both directions above some higher thresholds $\pm I_{th2}$ close to ± 30 mA we have reached a relatively stable and fully reproducible very-low-resistivity state (VLRS). The form of the $R_d(I_b)$ dependence in the VLRS is similar to that observed in LRS, compare Fig. 3(f) with Figs. 3(c) and 3(e). Nevertheless, the resistivity at zero current is much smaller than any previously recorded $R_d(0)$ and constitutes only about 50% of $R_d(0)$ from the pristine state. The broad resistivity minimum at $I_b=0$ is accompanied by high-resistivity-side “wings” at which R_d significantly exceeds all previously measured values.

The LRS and VLRS states exhibit memory effect in the sense that the system returns to the previously established resistivity state after a repeated current cycling. The memory of the VLRS is particularly strong, even with respect to the temperature cycling. VLRS is completely restored after thermal cycling above T_c and is only slightly modified after thermal cycling to room temperatures. Remarkably, the memory has not been fully erased even after maintaining the sample at room temperature for 48 h. Figure 4 shows the low-current part of the $R_d(I)$ dependence recorded for freshly created VLRS together with VLRS restored after maintaining the sample for two days at 300 K. The restored low-resistivity state seems to be less stable, in particular, for currents $I > 2$ mA, however, the major features of the VLRS are still preserved. The VLRS memory can be fully erased by biasing the sample at temperatures above T_c with a “depolarizing” ac current of an amplitude exceeding 1 mA. After the memory removal, VLRS converts into the pristine resistivity state.

The differences in the relative stability of various current-induced resistivity states can be clearly seen in Fig. 5, demonstrating $R_d(T)$ characteristics as recorded during the

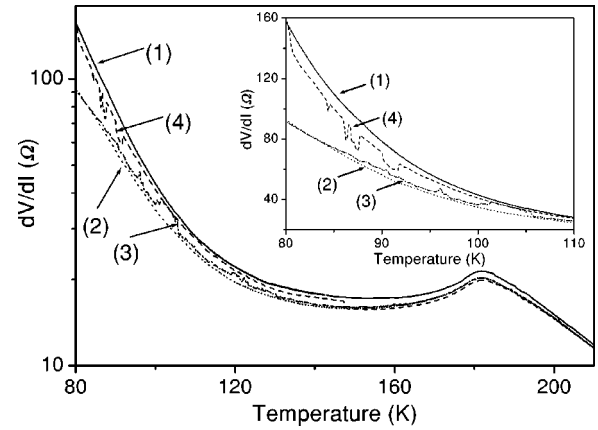


FIG. 5. Differential resistivity during the warm-up of a sample with zero bias current in different resistivity states; (1) pristine state, (2) freshly made VLRS, (3) VLRS after thermal cycling to room temperatures, (4) MRS state. The inset shows expanded view of the figure in the temperature range 80–110 K.

warm-up of different metastable states. The line marked (1) represents the characteristics obtained with a sample in the pristine high-resistivity state. The curve labeled (2) was recorded immediately after bias enforcement of a VLRS at 77 K. Remarkably, the VLRS resistivity stays well below the resistivity of the pristine state for all temperatures below $T_s = 225$ K. Above 225 K all characteristics almost coincide and no difference in the resistivity will be seen at room temperatures, despite the fact that the VLRS is memorized by the sample. The curve labeled (3) shows the resistivity during a warm-up cycle of a sample that has been driven into the VLRS state, warmed up to room temperatures, and cooled back to 77 K. Line (4) represents the warming-up process of the MRS state. The as-created VLRS and the pristine state are stable and exhibit smooth evolution of resistivity with increasing temperature. The restored VLRS and MRS are unstable and exhibit several back-and-forth resistance jumps between high and low resistivity. The high- and low-resistivity levels roughly coincide with resistivity in the pristine and freshly created VLRS. This is in a marked difference with the unidirectional resistivity jumps previously reported in $(\text{La}_{1-y}\text{Pr}_y)_{1-x}\text{Ca}_x\text{MnO}_3$ (LPCMO) systems.⁸ Warming-up characteristics of all current-created states start to converge around T_{min} and eventually fully coincide at $T > T_s$.

III. DISCUSSION

A. Temperature dependence of R_d

The resistivity versus temperature curves show three characteristic temperatures at which the dependence markedly changes. The less significant change, in the form of a shallow bent, occurs at $T_s = 225$ K. A similar feature in low-doped LSMO systems has been previously identified with the Jahn-Teller (JT) phase transition at which the high-temperature dynamic distortion becomes static resulting in establishing an orbital ordering.¹⁸ The next characteristic temperature is T_{max} at which the local resistivity maximum appears. At zero bias $T_{max}(I_b=0)$ coincides with the Curie temperature T_c

determined by magnetization measurements, and can be therefore associated with the onset of the ferromagnetic metallic conductivity. Above T_{max} the transport is dominated by the paramagnetic matrix, while below T_{max} the conductivity is dominated by the metallic ferromagnetic regions with aligned spins. However, at our doping level the ferromagnetic metallic state is not the ground state at low temperatures, which results in a shallow local minimum at the third characteristic temperature T_{min} followed by a resistivity upturning with decreasing temperature. The resistivity up-turn is a common feature in low-doped LCMO and LSMO systems. The temperature of the local minimum T_{min} is generally associated with a transition from the FM metallic state to the insulating FM phase with possible charge and/or orbital ordering.¹⁹

Manganites are extremely complicated systems and a variety of changing physical mechanisms control their behavior as the temperature is varied. In order to analyze the experimentally observed temperature dependence of the resistivity, it is convenient to divide the entire investigated temperature range into few subregions with different dominating conduction mechanisms. Following the temperature decrease we can distinguish a high-temperature paramagnetic-conductivity range at $T > T_c$, a metalliclike-percolation-conductivity region at $T_{min} < T < T_c$, and a low-temperature regime below T_{min} (77–150 K).

Hopping conductivity is the dominant conduction mechanism in the paramagnetic insulating state. Although small clusters of magnetic ions with aligned spins may exist in the paramagnetic state, nevertheless, the neighboring spins are only weakly correlated and metalliclike percolation conductivity is absent.^{1,2} Temperature dependence of the hopping conductivity in CMR systems is modeled either as hopping of small polarons or as Mott's variable-range hopping (VRH).^{1,2} The model of small polaron hopping predicts that²⁰

$$R_p(T) = R_0 T^\alpha \exp(E_g/kT), \quad (1)$$

where R_0 is a temperature independent coefficient, E_g is the activation energy, and k is the Boltzmann constant. Within an alternative VRH model²

$$R_p(T) = R_0 T \exp\left(\frac{T_0}{T}\right)^{1/4}. \quad (2)$$

Hopping in the VRH model is phonon assisted, therefore the prefactor R_0 depends on the phonon density. The temperature $T_0 = 18/kN(E_F)\xi^2$, where $N(E_F)$ is the density of states at the Fermi level and ξ is the localization length. Our experimental results can be reasonably well fitted to both formulas. Since the VRH model gives us a slightly better fit, particularly at temperatures approaching T_{max} , we have adopted Eq. (2) to analyze the experiment. We want to emphasize here that the temperature range of the paramagnetic state investigated in the experiment is rather restricted and we are not really able to choose between the alternative models for the hopping transport.

As a first stage we have fitted the paramagnetic-range resistivity measured at zero current to the VRH law (2). As

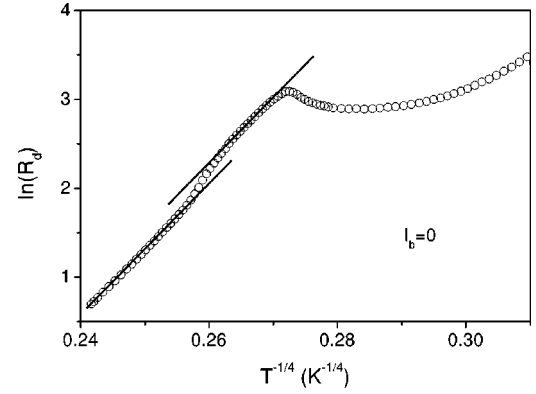


FIG. 6. Logarithm of the differential resistivity $R_d(T)$ as a function of $1/T^{0.25}$ in the paramagnetic-conductivity temperature range. Open symbols: experimental points. Solid lines: apparent fit to the variable-hopping model, see the text.

can be seen in Fig. 6 the fitting procedures result in two distinct temperature ranges, from room temperature down to 240 K and 185–220 K, where the resistivity obeys the VRH law and a transition region at $T \approx 225$ –230 K within which the R_0 prefactor in Eq. (2) slightly changes. The characteristic temperature $T_0 \approx 2.8 \times 10^7$ K obtained from the fitting procedures is compatible with T_0 values reported for other doped manganite systems.² A slight change in R_0 at the transition temperature T_s is plausible with changes in the phonon spectrum induced by the structural JT phase transition.

The phase diagram of LCMO determined by neutron-scattering measurements on crystals with various Ca^+ concentrations contains a structural transition within the paramagnetic insulating phase from the high-temperature pseudocubic to the low-temperature orthorhombic structure.²¹ Extrapolation of the experimental phase line into the low-doping levels reveals that the temperature of the structural transition at the doping level of our crystal, $x=0.18$, may be indeed close to $T_s=225$ K. Recent independent investigation of $\text{La}_{1-x}\text{Ca}_x\text{MnO}_3$ [with doping levels $0 < x < 0.15$ (Ref. 21) and $x=0.19$ (Ref. 22)] demonstrated that the temperature of the JT transition decreases with increasing Ca doping and for $x=0.19$, occurs at ≈ 150 K. We conclude therefore, that the discussed feature on the $R_d(T)$ curve may indeed correspond to the structural phase transition of the Jahn-Teller type.

The above conclusion requires an additional comment. It is apparent that JT ordering and metallic behavior are mutually exclusive. The resistivity at temperatures below the JT transition should abruptly increase, as was observed in LCMO with $x=0.19$.²² However, the resistivity of our sample evolves differently at temperatures below T_s . It was suggested that JT splitting of Mn^{3+} ions located close to the Ca ions is smaller than splitting of Mn^{3+} ions located around La ions.²³ Therefore, the energy needed to create a hole, Mn^{3+} -to- Mn^{4+} transition, in the vicinity of Ca ions is smaller. Thus, the concentration of Mn^{4+} cations around Ca ions results in the appearance of locally conducting ferromagnetic clusters.²⁴ In this scenario the long-range JT ordering transition and metalliclike conductivity at $T < T_c$ appear in phase-separated, spatially distinct regions of the sample.

At temperatures close to T_c the phase separation results in a coexistence of the insulating paramagnetic matrix and metallic ferromagnetic domains. At temperatures below T_{max} the ferromagnetic domains form percolating conducting paths. With decreasing temperature the strength of the percolation increases as the volume of the ferromagnetic phase increases. We find that the percolation conductivity follows the scaling law

$$R_m = R_{m0} \left(\frac{T^* - T}{T^*} \right)^{-\alpha}, \quad (3)$$

where α is the critical exponent and T^* is the temperature at which the concentration of the ferromagnetic phase corresponds to the percolation threshold.

The resistivity behavior around and below T_{max} can be well understood in the framework of recently proposed random-resistor percolation-network model, where a phase separated CMR manganite sample is represented by an effective resistance R_{eff} corresponding to a parallel connection of $R_m(T)$ and $R_p(T)$ resistances representing the ferromagnetic metallic and paramagnetic insulating phase, respectively.²⁴ We assume that R_m increases with increasing temperature according to Eq. (3), while $R_p(T)$ decreases with temperature according to Eq. (2). The competition between the hopping conductivity in the paramagnetic phase and metallic-percolation conductivity results in appearance of the local resistivity maximum at T_{max} .

By fitting our data to the two-resistor model, using Eq. (2) for R_p with parameters obtained from the previous fitting procedures for $T > T_{max}$, we find that the critical exponent $\alpha = 2.1 \pm 0.05$ and does not depend on the current flow, while the T^* at zero current is 190 ± 0.5 K and decreases with increasing current. Note that the critical exponent obtained from fitting the data to Eq. (3) is very close to $\alpha = 2$ predicted by the classical three-dimensional percolation theory for the conducting-phase-concentration scaling.²⁵

As shown in Fig. 7 the two-resistor model reasonably describes the resistivity around the peak and in the percolating region. However, the two-resistor model has been originally proposed to describe $R(T)$ of optimally doped manganites only.²⁴ Low-doped manganites operating close to the percolation threshold exhibit more complex behavior and the model has to be modified to account for the local R_d minimum at T_{min} and a subsequent resistivity up-turn with decreasing temperature.^{1,2} The resistivity up-turn in LCMO at low temperatures is generally ascribed to reentrance of an insulating phase at low temperatures.^{19,22} Nevertheless, in the existing literature there is no consensus about the possible low-temperature phase transition to the insulating state for the doping range of our samples.^{1,2,22}

A hint for searching the mechanism responsible for the resistivity up-turn at low temperatures is given by nonlinear I - V curves at low temperatures. At temperatures below T_{min} the pristine $R_d(I)$ characteristics becomes bell shaped and symmetric, see Fig. 2. The resistivity dependence on electric field in similar perovskite superconducting cuprates has been explained on the basis of the charge-transfer effects. Here the nonlinear data do not support the charge-transfer mechanism

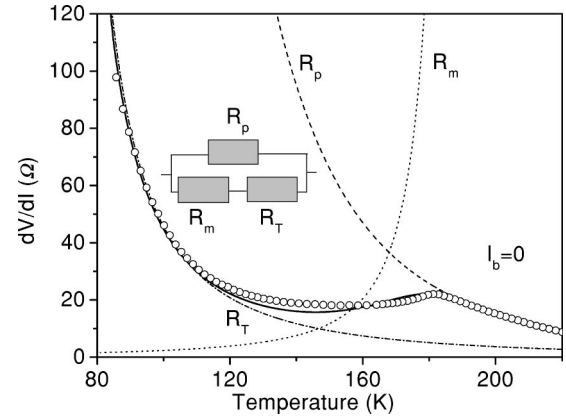


FIG. 7. General temperature behavior of the differential resistivity of $R_d(T)$ of $\text{La}_{0.82}\text{Ca}_{0.18}\text{MnO}_3$ single crystal in the framework of the three-resistor model shown schematically in the figure. Open symbol, experimental points; solid line, fit to the proposed three-resistor model; dashed line, R_p activated VRH conductivity in the paramagnetic range; dotted line, metallic-percolation conductivity obeying the critical scaling law; dash-dot line, tunnel conductivity that dominates at low temperatures.

but rather suggest the domination of the tunnel-conductivity mechanism below T_{min} . Although the absolute proof of the tunnel conductivity cannot be provided, we notice that the voltage dependence of $R_d(V)$ can be well fitted to the quadratic dependence, as predicted by the direct-tunnel-conductivity model,²⁶ or with even better accuracy to the Glasman and Matveev (GM) model of an indirect tunneling.²⁷ Similar nonlinear $R(V)$ dependencies have been observed in the magnetic multilayer systems containing explicit tunnel junctions between Sr- and La-doped manganites²⁸ and in $\text{La}_{2/3}\text{Ca}_{1/3}\text{O}_3$ films below Curie temperature²⁹ where conduction is dominated by the mesoscopic tunneling. The resistivity up-turn below T_{min} may be, therefore, attributed to the increasing contribution of the tunneling mechanism to the total conductivity with decreasing temperature.

With decreasing temperature the conducting percolation path becomes more and more interrupted by tunnel-type weak links. Simple modification to the two-resistor network model may account for the resistivity up-turn at low temperatures. When the percolation becomes more and more difficult the resistor representing a percolating path has to be replaced by a serial connection of two resistors representing metallic conductivity R_m and tunneling conductivity R_T , which is much higher than R_m and decreases in a nonlinear way with increasing current.

Preliminary magneto-optic measurements (MO) of our crystals revealed the existence of a network of twinning defects, similar to those observed in LCMO crystals prepared by the same technique and with almost the same doping level $x = 0.19$.²² The regular MO pattern of domains with opposite direction of magnetization appears in MO images at $T \sim T_{max}$ and becomes sharper and more pronounced at temperatures below T_{min} . Twinning defects and phase separation provide the reproducibility of the experimental data as the intrinsic tunneling weak links are prone to be localized at

such defects.³⁰ It is well known that in low-carrier-density manganites, band-bending effects in the vicinity of twin defects and grain boundaries result in depletion layers that act as localized insulating tunnel barriers.³⁰ As a consequence of the need to accommodate the lattice mismatch, tunnel barriers associated with twin-defect grain boundaries in perovskites are characterized by the high density of localized defect states. This will be even more pronounced in low-doped manganites systems where, as revealed by our MO investigations, magnetic domain walls appear at the twin defects. The band bending depends on the difference in magnetization between adjacent domains. Consistently with the observed $R_d(T)$ dependencies, the band-bending effects onset at $T=T_{max}$ and became significant at $T\sim T_{min}$ and below.³⁰ With decreasing temperature, the influence of the localized states becomes more pronounced. To describe properties of such barriers we refer to the (GM) model of an indirect tunneling.²⁷ The GM model has been recently successfully employed to describe the resistivity in bulk ceramic $\text{La}_{0.7}\text{Sr}_{0.3}\text{Mn}_{1-y}\text{Fe}_y\text{O}_3$ (Ref. 31) and in thin-film polycrystalline LCMO (Ref. 32) manganite systems, where tunnel conductivity appears in intergrain junctions. In our single-crystal case, the intrinsic tunnel junctions interrupting metallic percolation paths are spontaneously created at low temperature, most likely due to the band bending at twin grain boundaries.

In the GM model, temperature and voltage dependencies of the tunnel conductance are expressed as multistep tunneling via n localized states

$$G(V) = G_0 + \sum_{n=1}^{\infty} G_n(V, T), \quad (4)$$

where conductance G_0 represents the temperature-independent elastic-tunneling term while G_n describe tunneling through $n \geq 1$ localized states,

$$G_n(V) = a_n V^{n-2/(n+1)} \quad \text{for } eV \gg kT, \quad (5)$$

$$G_n(T) = b_n T^{n-2/(n+1)} \quad \text{for } eV \ll kT, \quad (6)$$

where coefficients a_n and b_n are exponential functions of the barrier thickness. For $R_d(I)$ curves presented in Fig. 2 the condition $eV \gg kT$ is fulfilled and we were able to fit the experimental $R_d(V)$ dependence to the GM model with only $n=2$ localized states.

$$1/R_T(V) = a_0 + a_1 + a_2 V^{4/3} + a_3 V^{5/2} + \dots \quad (7)$$

In the dynamic resistivity measurements at $I_b=0$ the condition $eV \ll kT$ is fulfilled and

$$1/R_T(T) = G_0 + G_1 + b_2 T^{4/3} + b_3 T^{5/2} + \dots \quad (8)$$

It has to be underlined at this point that we could equally well fit our experimental $R_T(T)$ to the equation describing the tunneling process with magnon emission or absorption by the tunneling electrons,³³

$$R_T = R_0 T \exp\left(\frac{E}{kT}\right). \quad (9)$$

Unfortunately, as in the case of the alternative models for the paramagnetic-regime resistivity, on the basis of currently available experimental data we are unable to really choose between the GM and the magnon-assisted tunneling model.

The behavior of resistivity of $\text{La}_{0.82}\text{Ca}_{0.18}\text{MnO}_3$ single crystal in the entire temperature range of the experiment can be thus described by extending the random-resistor network model to a set of three resistances R_p , R_m , and R_T . The equivalent three-resistor circuit, together with the measured and modeled $R_d(T)$ characteristics for $I_b=0$ is shown in Fig. 7. At $T > T_c$ the resistivity is governed by a hopping mechanism, $R_p \ll R_m$ and $R_T=0$. Around the local maximum $R_p \approx R_m$, while $R_T=0$ (no effective tunnel junctions exist yet). The parallel connection of R_p and R_m results therefore in a local R_d maximum. It should be noted that the experimentally observed increase of the resistivity value at T_{max} with increasing current follows directly from the characteristics shown in Fig. 7. At low temperatures R_p diverges and the competition between R_m and R_T results in the appearance of the local minimum and resistivity up-turn at low temperatures.

B. Bias current influence on $R_d(T)$

The current/electric-field influence on $R_d(T)$ is markedly different from the well-known effects of the application of the hydrostatic pressure or magnetic field.^{1,2} In the vicinity of T_{max} the applied pressure and magnetic field strongly reduce the resistivity and shift T_{max} to higher temperatures due to suppression of spin scattering of carriers. T_{min} in the low-doped regime, as was shown for LSMO systems, increases with increasing pressure and magnetic field.¹⁸ In our case, however, both T_{min} and T_{max} decrease with increasing current. In general, we notice that current starts to influence the resistivity at temperatures below T_s . Possible electric-field perturbation on JT distortion, which may produce electro-elastic effects influencing the conductivity in the paramagnetic phase, is practically negligible. At the same time the effects of perturbation of the oxygen octahedra by high pressure or a magnetic field result not only in an increase of T_{max} but also in a noticeable resistivity decrease in the temperature range between T_s and T_{max} .¹⁵ In general, the magnetic field interacts with the spin in the system and the electric field interacts with the induced polarization. Therefore, it is not surprising that the effects of such fundamentally different in nature interactions are different.

The electric field, or current, in general induces disorder that affect the insulating matrix and the ferromagnetic domains in different ways. Current-induced disorder prevents formation of a ferromagnetic phase at T_{max} and thus extends the paramagnetic phase range towards lower temperatures. This effect is due to the fact that the self-field of the current is directed in different directions at the positions of magnetic Mn ions surrounding the current path. Indeed, our analysis performed in the framework of the proposed three-resistor model shows that with increasing current, the parameters in Eq. (2) and the critical exponent α in Eq. (3) do not change, while the threshold temperature T^* decreases with increasing current.

At low temperatures, current-induced disorder melts the charge-ordered insulating phase and enhances the range of the ferromagnetic metallic phase.^{5,7,8} Alternatively, in the tunnel scenario, current flow imposes dc voltage bias on the intrinsic tunnel junctions and thus reduces the tunnel conductivity leading to an effective reduction of T_{min} . The direction of the shift of the characteristic temperatures T_{min} and T_{max} depends on the properties of the CMR system. In LPCMO and LSMO systems, the charge-order transition temperature T_{co} associated with T_{min} is higher than the ferromagnetic-transition temperature T_c associated with T_{max} . In LPCMO and LSMO systems, current-induced melting of the charge-ordered state results in an effective increase of T_{max} accompanied by a resistivity decrease at the transition point. In LCMO T_c is higher than the temperature of the insulating-phase onset and, therefore current-induced melting of the insulating phase causes a decrease in T_{min} with a simultaneous increase of the resistivity for temperatures between T_{min} and T_{max} , as observed in our experiments. At the same time, the current-induced disorder prevents formation of the ferromagnetic phase close to T_{max} , which results in decrease of T_{max} with increasing current, accompanied by the resistivity increase. The electric-field effect is opposite to the magnetic field and pressure effect, which enhance the spin ordering and formation of the magnetically ordered phase.

C. Resistivity switching and metastable states

The most intriguing results of our experiments are transitions to the low-resistivity metastable states and the fact that such transition requires a bipolar current sweep; dc current ramp in one direction only is not sufficient. Although we do not have a complete understanding of the underlying physical mechanism we may think about several plausible scenarios leading to the switching to metastable states with memory.

Current-induced instabilities and resistivity jumps observed in our experiments closely resemble effects associated with current-induced resistivity switching in artificial magnetic multilayers.³⁴ In such systems current-induced resistivity jumps result from spin-polarized current-induced switching of magnetic moments between parallel and antiparallel orientations, the latter having a higher resistance than the former one.^{34–36} MO images of our sample show that regions adjacent to the twin-defect tunnel junction have, in general, an opposite magnetic polarization. These magnetically ordered regions may act as ferromagnetic electrodes in a spin-polarized tunneling arrangement in which the tunnel barrier plays the role of a spacer. The electrons moving between the magnetic metallic domain separated by a nonmagnetic spacer become spin polarized by the local moment of the first domain. These electrons tends to align the magnetic moment in the second domain to the direction parallel to their own spin polarization.^{34–41} The switching of the magnetic moment occurs at sufficiently high intensity of spin-polarized current exceeding some threshold current.

Recently, current-induced switching of magnetic moments and resistivity jumps have been also observed in artificial manganite trilayers.^{36,37} Evidently, our experimentally ob-

served picture is more complex and contains considerably more jumps and switches than observed in simple artificial structures.^{34,36,37} It is easy to imagine that the percolating filament contains not just one but several active tunnel junctions, and that the global percolation path is constituted by several parallel and/or braiding filaments.

To switch the polarization of the magnetization by means of the spin-polarized current, the current density has to exceed a critical value j_c . In artificial Co-based spin-transfer systems the experimentally determined critical current densities are very high.³⁴ The threshold current in the spin-transfer model is proportional to the anisotropy constant K .³⁸ Anisotropy constant of cobalt, $K=1.5\times 10^5$ J/m³, provides critical current densities of the order of 10^6 – 10^7 A/cm², in good agreement with the experiments.³⁴ The magnetic anisotropy in our crystal is about two orders of magnitude smaller and the effects of current-induced switching can be obtained at sufficient lower current densities. Assuming that the PS ferromagnetic domains have the size of the order of a fraction of a micrometer we may evaluate the size of a typical weak link in the percolation path to be below 0.1 μ m. This makes the switching plausible since the required current densities fall to a reasonably low current level of the order of 10 mA, similar to the threshold current observed in the experiments.

The simple application of a spin-transfer model does not explain many features of the metastable states, and in particular, cannot account for a subsequent transition into VLRS at currents exceeding the second threshold. As already mentioned, in the metastable resistivity states we have observed several random telegraph switchings of resistivity with bias-dependent amplitudes and lifetimes. As shown by our first analysis it is not the current but the voltage that determines the dynamics of the switching phenomena. This feature guided us to the conclusion that the nature of the telegraph switching is of the electric rather than magnetic origin.¹⁷ Extending this scenario we may associate resistivity switching with opening of additional channels for the spin-polarized tunneling with increasing voltage bias across the tunnel junction. These additional channels may simply reflect the structure of the real density of states (DOS) in the tunnel electrodes. CMR manganites are known to be characterized by almost 100% spin polarization and the majority and minority electron bands are separated by an energy gap of the order of 0.7–1.5 eV.^{40,42} It is well known that the tunnel conductivity $dI/dV=1/R_d$ is proportional to the density-of-states function. The major features in the DOS for a LCMO system determined by means of photospectroscopy correspond to the voltage positions of major peaks and valleys in the R_d dependence.

D. Memory effects

The memory effect observed in our experiments are partially similar to the memory effect observed in charge-ordered Nd_{0.5}Sr_{0.5}MnO₃ single crystals and LPCMO thin films, where the applied electric field/current melts charge-ordered clusters, establishes a percolative conductive path, and thus dramatically decreases the resistivity.^{8,43} The low-

resistivity state reverts to the initial high-resistivity state only after being kept for a few days at room temperature.⁴³

The persistence of the low-resistivity state in our samples after thermal cycling to room temperatures indicates that the memory must be associated with some structural changes in the crystalline structure. The depletion layers at grain boundaries are very thin, of the order of 1 nm,³⁰ therefore, at the bias level employed in the experiment we reach extremely high values of the electric fields in the tunnel barrier. Manganites are strongly inhomogeneous compounds and high electric field acting in the space between two neighboring metallic domains may produce a transformation in the crystal lattice. Since a sufficient electrical field can change the crystal and local symmetry of the ions and strongly influence the electronic state of Jahn-Teller centers, substantial magneto-electric effects can also be expected.⁴⁴ The stress imposed from the surrounding bulk may prevent the local cluster from fast relaxation to the initial state. As a result, the VLRS is robust and persists even after thermal cycling to room temperatures. As pointed out by Uehara and Cheong the energy barrier separating structurally phase-separated states in LCMO is of the order of 450 K, which may lead to the above-described memory effects.¹⁶

IV. CONCLUSIONS

In conclusion, we have investigated the temperature behavior of the dynamic resistivity of a low-doped $\text{La}_{0.82}\text{Ca}_{0.18}\text{MnO}_3$ single crystal polarized with different currents. The experiments have revealed that the dc current can enforce pronounced resistivity jumps and create various metastable low-resistivity states in the investigated system, even in the absence of applied magnetic field. To create a metastable resistivity state a specific procedure of a bipolar current ramp, exceeding some threshold current is required. There are at least two threshold currents in the investigated systems; exceeding the higher one results in the creation of a relatively stable very-low-resistivity state with memory that persists even after thermal cycling to room temperatures.

Detailed analysis of the temperature dependence of the resistivity suggests that at high temperatures, where the LCMO sample is in the paramagnetic state the dominant conduction mechanism is the variable-range hopping of polarons. A possibility of a structural Jahn-Teller transition within the paramagnetic temperature range and its influence on the transport properties has been examined. At temperatures close to MI (metal-insulator) transition, metallic-percolation conductivity through phase-separated ferromagnetic domains starts to compete with the polaron-hopping conductivity. The metallic-percolation conductivity obeys the

scaling law. With lowering temperature the percolation becomes hindered by appearance of intrinsic tunnel junctions, associated with structural twin defects in the crystal. The tunnel conductivity follows predictions of the indirect-resonant-tunneling model with $n=2$ inelastic channels, as well as the model of magnon-assisted tunneling. At this stage of the experiments we were unable to choose between the alternative tunneling models.

The temperature behavior of the resistivity of low-doped LCMO has been successfully described in the framework of a three-resistor model developed as an extension of the existing random two-resistor network. The equivalent resistivity in our model is presented as a parallel-serial connection of three resistors representing hopping, metallic, and tunnel conductivity.

The influence of current on the temperature dependence of the resistivity manifests itself in shifts of the local resistivity maximum and minimum, as well as in changes of the resistivity measured at these characteristic points. The observed behavior is consistent with the predictions of the proposed three-resistor model.

The peculiar behavior of current-induced metastable resistivity states can be tentatively understood in the framework of spin-polarized transfer theory. Spin-polarized current flow across intrinsic twin-boundary tunnel junctions separating neighboring ferromagnetic domains with opposite orientation of magnetic moments may lead to current-enforced switching of the domain arrangement into a magnetic-moment configuration with much lower resistivity. The presence of peaks and valleys in the resistivity vs bias characteristics has been tentatively interpreted as a manifestation of the density-of-states structure in the ferromagnetic electrodes, available at a given voltage bias across the junction for the tunneling of spin-polarized electrons. Although we do not have a complete picture of the physics involved in the creation and performance of the metastable resistivity states we hope that our experiments will provide a stimulus for more theoretical and experimental work that will shed light on this fascinating phenomenon.

ACKNOWLEDGMENTS

This research was supported by the Israeli Science Foundation administered by the Israeli Academy of Sciences and Humanities (Grant No. 209/01). The assistance of Professor Yeshurun and Dr. Mandel in magneto-optics investigations is greatly appreciated. X-ray analysis of LCMO crystals was performed by Dr. Mogylanski. Ya.M.M. and D.A.S. were supported by the Russian Foundation for Basic Research Project No. 16280.

*Also at Instytut Fizyki PAN, Al. Lotników 32, PL 02-668 Warszawa, Poland.

¹E. Dagotto, T. Hotta, and A. Moreo, *Phys. Rep.* **344**, 1 (2001).

²J.M.D. Coey, M. Viret, and S. von Molnar, *Adv. Phys.* **48**, 167 (1999).

³M. Fiebig, K. Miyano, Y. Tomioka, and Y. Tokura, *Science* **280**, 1925 (1998); V. Ponnambalam, S. Parashar, A. R. Raju, and

C.N.R. Rao, *Appl. Phys. Lett.* **74**, 206 (1999); S. Parashar, E.E. Ebenso, A.R. Raju, and C.N.R. Rao, *Solid State Commun.* **114**, 295 (2000).

⁴T. Wu, S.B. Ogale, J.E. Garrison, B. Nagaraj, Z. Chen, R.L. Greene, R. Ramesh, T. Venkatesan, and A.J. Millis, *Phys. Rev. Lett.* **86**, 5998 (2001); H. Oshima, K. Miyano, Y. Konishi, M. Kawasaki, and Y. Tokura, *Appl. Phys. Lett.* **75**, 1473 (1999).

- ⁵J. Stankiewicz, J. Sese, J. Garcia, J. Blasco, and C. Rillo, *Phys. Rev. B* **61**, 11 236 (2000).
- ⁶S. Srivastava, N.K. Pandey, P. Padhan, and R.C. Budhani, *Phys. Rev. B* **62**, 13 868 (2000).
- ⁷A. Asamitsu, Y. Tomioka, H. Kuwahara, and Y. Tokura, *Nature (London)* **388**, 50 (1997).
- ⁸N.A. Babuschkina, L.M. Belova, D.I. Khomskii, K.I. Kugel, O.Yu. Gorbenko, and A.R. Kaul, *Phys. Rev. B* **59**, 6994 (1999).
- ⁹L.P. Gor'kov and V.Z. Kresin, *J. Supercond.* **13**, 239 (2000).
- ¹⁰I. Kim, J. Dho, and S. Lee, *Phys. Rev. B* **62**, 5674 (2000); V. Chechersky, A. Nath, I. Isaak, J.P. Franck, K. Ghosh, H. Ju, and R.L. Greene, *ibid.* **59**, 497 (1999).
- ¹¹R. De Renzi, G. Allodi, G. Amoretti, M.C. Guidi, S. Fanesi, G. Guidi, F. Licci, I. Caneiro, F. Prado, R. Sanches, S. Oseroff, and A. Amato, *Physica B* **289-290**, 85 (2000).
- ¹²S.G. Barsov, A.L. Getalov, V.P. Koptev, S.A. Kotov, S.M. Mikirtychants, G.V. Shcherbakov, A.A. Arsenov, and Ya.M. Mukovskii, *Physica B* **289-290**, 81 (2000).
- ¹³M. Uehara, S. Mori, C.H. Chen, and S.-W. Cheong, *Nature (London)* **399**, 560 (1999); M. Fath, S. Freisem, A.A. Menovsky, Y. Tomioka, J. Aarts, and J.A. Mydosh, *Science* **285**, 1540 (1999); P.G. Radaelli, R.M. Ibberson, D.N. Arguriou, H. Casalta, K.H. Andersen, S.-W. Cheong, and J.F. Mitchell, *Phys. Rev. B* **63**, 172419 (2001); Q. Lu, C.-C. Chen, and A. de Lozanne, *Science* **276**, 2006 (1997).
- ¹⁴D.A. Shulyatev, A.A. Arsenov, S.G. Karabashev, and Ya.M. Mukovskii, *J. Cryst. Growth* **198/199**, 511 (1999).
- ¹⁵V. Markovich, E. Rosenberg, Y. Yuzhelevski, G. Jung, G. Gorodetsky, D.A. Shulyatev, and Ya.M. Mukovskii, *Appl. Phys. Lett.* **78**, 3499 (2001).
- ¹⁶M. Uehara and S.-W. Cheong, *Europhys. Lett.* **52**, 674 (2000).
- ¹⁷Y. Yuzhelevski, V. Dikovskiy, V. Markovich, G. Gorodetsky, G. Jung, D. Shulyatev, and Ya.M. Mukovskii, *Fluct. Noise Lett.* **1**, L105 (2001).
- ¹⁸B. Martinez, R. Senis, L. Balcells, V. Laukhin, J. Fontcuberta, L. Pinsard, and A. Revcolevschi, *Phys. Rev. B* **61**, 8643 (2000).
- ¹⁹Y. Moritomo, A. Asamitsu, and Y. Tokura, *Phys. Rev. B* **56**, 12 190 (1997); T. Okuda, Y. Tomioka, A. Asamitsu, and Y. Tokura, *ibid.* **61**, 8009 (2000).
- ²⁰T. Holstein, *Ann. Phys. (N.Y.)* **8**, 325 (1959).
- ²¹G. Biotteau, F. Moussa, M. Hennion, J. Rodriguez-Carvajal, A. Wildes, L. Pinsard, and A. Revcolevschi, *Physica B* **276-278**, 562 (2000).
- ²²B.B. van Aken, A. Meetsma, and T.T.M. Palstra, *cond-mat/0105197* (unpublished); B.B. van Aken, A. Meetsma, and T.T.M. Palstra, *cond-mat/0103628* (unpublished).
- ²³J. Alonso, E. Herrero, J.M. Gozalez-Calbet, M. Vallet-Regi, J.L. Martinez, J.M. Rojo, and A. Hernando, *Phys. Rev. B* **62**, 11 328 (2000).
- ²⁴M. Mayr, A. Moreo, J. Verges, J. Arispe, A. Feiguin, and E. Dagotto, *Phys. Rev. Lett.* **86**, 135 (2001).
- ²⁵A. Efros and B. Shklovskij, *Electronic Properties of Disordered Conductors* (Springer, New York, 1984).
- ²⁶J.G. Simmons, *J. Appl. Phys.* **34**, 1793 (1963).
- ²⁷L.I. Glazman and K.A. Matveev, *Zh. Eksp. Teor. Fiz.* **94**, 332 (1988) [*Sov. Phys. JETP* **67**, 1276 (1988)].
- ²⁸H.Q. Yin, J.S. Zhou, K. Sugawara, and J.B. Goodenough, *J. Magn. Magn. Mater.* **222**, 115 (2000); M. Viret, M. Drouet, J. Nassar, J.P. Contour, C. Fermon, and A. Fert, *Europhys. Lett.* **39**, 545 (1997); M.H. Jo, N.D. Mathur, N.K. Todd, and M.G. Blamire, *Phys. Rev. B* **61**, R14 905 (2000).
- ²⁹W. Westerburg, F. Martin, S. Friedrich, M. Maier, and G. Jakob, *J. Appl. Phys.* **86**, 2173 (1999); P. Reutler, A. Bensaid, F. Herbstritt, C. Hofener, A. Marx, and R. Gross, *Phys. Rev. B* **62**, 11 619 (2000).
- ³⁰J. Klein, C. Hofener, S. Uhlenbruck, L. Al, B. Buchner, and R. Gross, *Europhys. Lett.* **47**, 371 (1999).
- ³¹K.B. Chashka, B. Fisher, J. Genossar, L. Patlagan, G.M. Reisner, and E. Shimshoni, *Phys. Rev. B* **63**, 064403 (2001).
- ³²M. Ziese, *Phys. Rev. B* **60**, R738 (1999).
- ³³S. Zhang, P.M. Levy, A.C. Marley, and S.S.P. Parkin, *Phys. Rev. Lett.* **79**, 3744 (1997); X.-F. Han, A.C.C. Yu, M. Oogane, J. Murai, T. Daibou, and T. Miyazaki, *Phys. Rev. B* **63**, 224404 (2001).
- ³⁴E.B. Myers, D.C. Ralph, J.A. Katine, R.N. Louie, and R.A. Buhrman, *Science* **285**, 867 (1999); E.B. Myers, D.C. Ralph, J.A. Katine, F.J. Albert, and R.A. Buhrman, *J. Appl. Phys.* **87**, 5502 (2000); J.A. Katine, F.J. Albert, and R.A. Buhrman, *Appl. Phys. Lett.* **76**, 354 (2000).
- ³⁵J. Slonczewski, *J. Magn. Magn. Mater.* **159**, L1 (1996).
- ³⁶J.Z. Sun, *J. Magn. Magn. Mater.* **202**, 157 (1999).
- ³⁷M.H. Jo, N.D. Mathur, J.E. Evetts, and M.G. Blamire, *Appl. Phys. Lett.* **77**, 3803 (2000); H.Q. Yin, J.S. Zhou, K. Sugawara, and J.B. Goodenough, *J. Magn. Magn. Mater.* **222**, 115 (2000).
- ³⁸C. Heide, P.E. Zilberman, and R.J. Elliot, *Phys. Rev. B* **63**, 064424 (2001).
- ³⁹M. Julliere, *Phys. Lett.* **54A**, 225 (1975).
- ⁴⁰J.M. de Teresa, A. Barthelemy, J.P. Contour, and A. Fert, *J. Magn. Magn. Mater.* **211**, 160 (2000).
- ⁴¹J.C. Slonczewski, *Phys. Rev. B* **39**, 6995 (1989).
- ⁴²J.Y.T. Wei, N.C. Yeh, and R.P. Vasquez, *Phys. Rev. Lett.* **79**, 5150 (1997).
- ⁴³T. Mori, *Phys. Rev. B* **58**, 12 543 (1998).
- ⁴⁴M. D. Kaplan and B. G. Vekhter, *Cooperative Phenomena in Jahn-Teller Crystals* (Plenum Press, New York, 1995).